Published in final edited form as:
Ophthalmology. 2013 March ; 120(3): 535–543. doi:10.1016/j.ophtha.2012.09.055.

Enhanced Detection of Open-angle Glaucoma with an Anatomically Accurate Optical Coherence Tomography–Derived Neuroretinal Rim Parameter

Balwantray C. Chauhan, PhD[1], **Neil O'Leary, PhD**[1], **Faisal A. AlMobarak, MD**[1,2], **Alexandre S. C. Reis, MD**[1,3], **Hongli Yang, PhD**[4], **Glen P. Sharpe, MSc**[1], **Donna M. Hutchison, BSc**[1], **Marcelo T. Nicolela, MD**[1], and **Claude F. Burgoyne, MD**[4]

[1]Department of Ophthalmology and Visual Sciences, Dalhousie University, Halifax, Nova Scotia, Canada

[2]Department of Ophthalmology, College of Medicine, King Saud University, Riyadh, Saudi Arabia

[3]Department of Ophthalmology, University of São Paulo, São Paulo, Brazil

[4]Devers Eye Institute, Portland, Oregon

Abstract

Objective—Neuroretinal rim assessment based on the clinical optic disc margin (DM) lacks a sound anatomic basis for 2 reasons: (1) The DM is not reliable as the outer border of rim tissue because of clinically and photographically invisible extensions of Bruch's membrane (BM) inside the DM and (2) nonaccountability of rim tissue orientation in the optic nerve head (ONH). The BM opening-minimum rim width (BMO-MRW) is a parameter that quantifies the rim from its true anatomic outer border, BMO, and accounts for its variable orientation. We report the diagnostic capability of BMO-MRW.

Design—Case control.

Participants—Patients with open-angle glaucoma (n = 107) and healthy controls (n = 48).

Methods—Spectral-domain optical coherence tomography (SD-OCT) with 24 radial and 1 circumpapillary B-scans, centered on the ONH, and confocal scanning laser tomography (CSLT) were performed. The internal limiting membrane (ILM) and BMO were manually segmented in each radial B-scan. Three SD-OCT parameters were computed globally and sectorally: (1) circumpapillary retinal nerve fiber layer thickness (RNFLT); (2) BMO-horizontal rim width (BMO-HRW), the distance between BMO and ILM in the BMO reference plane; and (3) BMO-MRW, the minimum distance between BMO and ILM. Moorfields Regression Analysis (MRA) with CLST was performed globally and sectorally to yield MRA1 and MRA2, where "borderline" was classified as normal and abnormal, respectively.

Main Outcome Measures—Sensitivity, specificity, and likelihood ratios (LRs) for positive and negative test results (LR+/LR−).

Results—The median (interquartile range) age and mean deviation of patients and controls were 69.9 (64.3–76.9) and 65.0 (58.1–74.3) years and −3.92 (−7.87 to −1.62) and 0.33 (−0.32 to 0.98) dB, respectively. Globally, BMO-MRW yielded better diagnostic performance than the other parameters. At 95% specificity, the sensitivity of RNFLT, BMO-HRW, and BMO-MRW was

Correspondence: Balwantray C. Chauhan, PhD, Department of Ophthalmology and Visual Sciences, Dalhousie University, 1276 South Park St., 2W Victoria, Halifax, Nova Scotia, Canada B3H 2Y9. bal@dal.ca.

70%, 51%, and 81%, respectively. The corresponding LR+/LR− was 14.0/0.3, 10.2/0.5, and 16.2/0.2. Sectorally, at 95% specificity, the sensitivity of RNFLT ranged from 31% to 59%, of BMO-HRW ranged from 35% to 64%, and of BMO-MRW ranged from 54% to 79%. Globally and in all sectors, BMO-MRW performed better than MRA1 or MRA2.

Conclusions—The higher sensitivity at 95% specificity in early glaucoma of BMO-MRW compared with current BMO methods is significant, indicating a new structural marker for the detection and risk profiling of glaucoma.

The clinically identified optic disc margin (DM) has conventionally been thought to represent the inner edge of Elschnig's ring or border tissue.[1] Anatomically, border tissue is a circular band of connective tissue that fuses the sclera to Bruch's membrane (BM) forming the blood–brain barrier to isolate the choroid from the retinal ganglion cell axons in the optic nerve head (ONH). The clinical DM and optic disc cup are clinical constructs that are thought to delineate the outer and inner borders of the neuroretinal rim, respectively, and are critical components of the fundoscopic examination in individuals assessed for glaucoma.

We recently co-localized stereo optic disc photographs to spectral-domain optical coherence tomography (SD-OCT) data such that we could precisely identify locations in an SD-OCT radial B-scan that corresponded to features in the disc photograph.[2,3] We reported 3 findings that have a practical bearing on the accuracy of current neuroretinal rim assessment. First, the clinically identified DM is rarely a single anatomic structure or an identifiable junction, such as the inner edge of border tissue.[2] In most eyes it corresponds variably to multiple anatomic structures in SD-OCT images. Second, in some regions of all ONHs, BM extends internally beyond the clinically identified DM (toward the center of the ONH) and is both clinically and photographically invisible. Because the outer border of the rim is the termination of BM in these areas and not the more external DM, the rim is narrower than that with clinical or photographic evaluation. Third, because clinical, photographic, or confocal scanning laser tomography (CSLT)-based rim width measurements are made in the plane of the perceived DM without reference to the orientation of the rim tissue, for the same number of axons, the rim width will be greater in cases where the orientation of the rim tissue is more horizontal (e.g., in the temporal sector of tilted optic discs) compared with when it is more perpendicular.[3] The optic disc photographs and SD-OCT radial B-scans of all 40 subjects analyzed illustrating these 3 findings are available online (http://ophthalmology.medicine.dal.ca/research/onh.html, accessed May 26, 2012).

Taken together, these observations indicate that the basis of current rim measurements lacks a solid anatomic foundation. We reasoned that the termination of BM, or Bruch's membrane opening (BMO), is a logical anatomic outer border of the rim. Although rim width measurement based on BMO has been proposed,[4–6] identification of BMO was performed primarily for the automated detection of the DM and to derive a rim measurement that mimics current clinical evaluation.[4,7] Currently with SD-OCT, this measurement is made along the BMO reference plane, which is approximately a horizontal planar surface. We therefore termed this parameter "BMO-horizontal rim width" (BMO-HRW).[3] In addition, several investigators have recognized that measurements should account for the orientation of the rim tissue relative to the point of measurement[8–10] and have argued for measuring the minimum distance from BMO to the internal limiting membrane (ILM). Although its terminology has varied in past descriptions,[8–10] in a recent report we adopted the term BMO minimum rim width (BMO-MRW) for this parameter and provided a quantitative analysis supporting the rationale for such a measurement.[3]

Rim width estimates based on the DM vary regionally and significantly from those based on BMO.[3] The purpose of this study was to determine whether SD-OCT rim parameters that are based on BMO (i.e., BMO-HRW and BMO-MRW) can better identify patients with

glaucoma from healthy subjects compared with ones based on the DM obtained with CLST. Because SD-OCT circumpapillary retinal nerve fiber layer thickness (RNFLT) measurements are made approximately perpendicular to the orientation of the axons (that is where the RNFLT measurement is at a minimum), we also wanted to compare the ability of RNFLT to BMO-MRW in distinguishing healthy eyes from those with early glaucoma.

Materials and Methods

Participants

Study participants included patients with open-angle glaucoma and healthy normal controls. The subjects were recruited from 3 prospective longitudinal observational studies being carried out at the Eye Care Centre, Queen Elizabeth II Health Sciences Centre, Halifax, Nova Scotia, Canada. At each study visit, subjects had a variety of imaging and perimetric tests performed. If both eyes were eligible, 1 eye was randomly selected as the study eye. The study was approved by the Ethics Review Board of the QEII Health Sciences Centre. In accordance with the Declaration of Helsinki, all subjects gave informed consent to participate.

For patients, inclusion criteria were (1) diagnosis of open-angle glaucoma, including primary, pseudoexfoliative, or pigmentary glaucoma; (2) previously documented evidence of progressive ONH changes judged clinically with stereo-disc photography or previously published criteria with CSLT in which the size and depth of clusters of pixels that have undergone significant change from the baseline are evaluated;[11,12] (3) a positive Glaucoma Hemifield Test[13] with standard automated perimetry (Swedish Interactive Thresholding Algorithm[14] program 24-2 of the Humphrey Field Analyzer [Carl Zeiss Meditec, Dublin, CA]); and (4) best-corrected visual acuity ≥0.3 (20/40) logarithm minimum angle of resolution in the study eye. Exclusion criteria were (1) concomitant ocular disease and systemic medication known to affect the visual field and refractive error exceeding ±6.00 diopters sphere or ±3.00 diopters astigmatism.

For healthy controls, inclusion criteria were (1) normal eye examination with intraocular pressure less than 21 mmHg; and (2) normal visual field, defined as a Glaucoma Hemifield Test, mean deviation, and pattern standard deviation within normal limits. The exclusion criterion was refractive error exceeding ±6.00 diopters sphere or ±3.00 diopters astigmatism. Only reliable visual field examinations as judged by the perimetrist's notes, which took into account the automated reliability indices, were used.

Imaging

All subjects had their study eye imaged with both SD-OCT (Spectralis, Heidelberg Engineering GmbH, Heidelberg, Germany) and CSLT (Heidelberg Retina Tomograph, Heidelberg Engineering GmbH) on the same day.

Two scanning patterns were used with SD-OCT. First, a radial pattern comprising 24 angularly equidistant high-resolution 15-degree B-scans was used to compute the neuroretinal rim parameters. The scan pattern was centered on the ONH, and data for each B-scan were averaged from 20 to 30 individual B-scans, with 768 A-scans per B-scan. Second, a 12-degree circular scan was used to measure the circumpapillary RNFLT. The scan comprised 1536 A-scans centered on the ONH, and data were averaged from 16 individual B-scans. The internal image registration and tracking software that significantly reduces the effects of eye movements[15] was used.

With CSLT, a 15-degree scan pattern comprising 16 confocal sections (with a transverse sampling of 384×384 pixels) per millimeter of scan depth was used to image the ONH. The

mean topography and reflectance images were automatically computed by the software from 3 respective individual images.

With each technique, the operator checked for image quality, including with SD-OCT proper B-scan positioning in the image frame, centration on the ONH, and quality score >20. When necessary, images were reacquired.

Image Segmentation

The SD-OCT raw data were imported into customized software based on the Visualization Toolkit (VTK, Clifton Park, NY), which enables segmentation of ONH structures in the B-scan with simultaneous projection in the infrared image.[16,17] One trained observer (F.A.A.) segmented the ILM and the 2 BMO points in each B-scan. The 3-dimensional coordinates of these structures were then used to calculate the SD-OCT–based neuroretinal rim parameters (see below). All data were transformed to right eye format.

The same observer segmented the optic DM in the CSLT reflectance image. In each case, the infrared image with SD-OCT also was used as a guide to identify the DM in the CSLT image. The DM was defined as the innermost border of reflective tissue that was internal to any pigmented tissue (if present) and within which only neural tissue was present.

Neuroretinal Rim Parameters

The BMO-based neuroretinal rim parameters have been detailed by Reis et al[3] and are illustrated in Figure 1. Briefly, the 24 radial scans yielded 48 BMO points with 3-dimensional coordinates through which were fitted (1) a spline to derive a closed curve representing the BMO around the ONH from which BMO area was computed and (2) a best-fit plane representing the BMO reference plane. The BMO-HRW was defined as the distance between the projection of BMO to the BMO reference plane and the ILM, along the BMO reference plane (Fig 1). The BMO-HRW is deliberately designed to be equivalent to measurements recently described with SD-OCT.[4–6] The BMO-MRW was defined as the minimum distance between the BMO and the ILM. Both BMO-HRW and BMO-MRW were computed at the 48 equally spaced angular positions around the BMO center.

Internal software (Heidelberg Eye Explorer, Heidelberg Engineering GmbH) was used to generate the results of the Moorfields Regression Analysis (MRA)[18] with CSLT. The MRA uses the relationship between the optic disc area and the neuroretinal rim area in healthy subjects and classifies the rim as being within normal limits (if the rim area is within the 95% prediction interval for the given disc area), borderline (if the rim area is within the 99% prediction interval), and outside normal limits (if the rim area is outside the 99.9% prediction interval).

Data Analysis

The SD-OCT neuroretinal rim parameters were computed as means globally and for the four 45-degree sectors (superonasal, inferonasal, inferotemporal, and superotemporal) and the two 90-degree sectors (nasal and temporal). The circumpapillary RNFL was segmented according to the internal software, checked for accuracy, and corrected when necessary. The raw values were then extracted, and the global and sectoral circumpapillary RNFLT values were computed. Finally, the respective global and sectoral MRA results from CSLT also were extracted from the internal software.

The diagnostic performance of RNFLT, SD-OCT rim parameters, and MRA were compared with receiver operating characteristic (ROC) analysis globally and sectorally. Because the MRA yields a “borderline” classification, 2 MRA criteria were used: (1) conservative,

MRA1, where the borderline cases were classified as normal; and (2) liberal, MRA2, where borderline cases were classified as abnormal. Thus, there were 2 discrete points for the MRA analysis on the ROC curve, whereas for the other parameters, the sensitivity and specificity values were computed for all possible cutoff values of the respective parameters.

Likelihood ratios (LRs) for positive (the odds that a positive result would be expected from a patient with glaucoma compared with control) or negative (the odds that a negative result would be expected from a patient with glaucoma compared with control) test results for RNFLT, BMO-HRW, and BMO-MRW based on the sensitivity at a fixed specificity of 95% were computed. The LRs were then used to derive posttest probability values based on varying pretest probabilities.[19] Because the MRA does not yield a range of possible cutoff values to derive sensitivity at fixed specificity, only MRA1 was used.

Group variables were compared with the *t* test. Associations between variables were examined with the Pearson correlation coefficient.

Results

There were 107 patients with glaucoma and 48 healthy controls in the study; their median (interquartile range) ages were 70.3 years (64.3–76.9 years) and 65.0 years (58.1–74.3 years), respectively, and the mean deviations of the visual field obtained on the same day as the imaging were −3.92 (−7.87 to −1.62) and 0.33 (−0.32 to 0.98) dB, respectively. Summary SD-OCT parameters are shown in Table 1. There was a significant difference between patients and controls for all the parameters investigated ($P < 0.01$).

In control subjects, global BMO-MRW was weakly associated with age, reaching borderline significance ($r = -0.26$, $P = 0.08$). This association was stronger compared with that between global BMO-HRW and age ($r = -0.06$, $P = 0.70$; Fig 2). Likewise, the relationship between global BMO-MRW and BMO area was stronger ($r = -0.46$, $P<0.01$) compared with global BMO-HRW and BMO area ($r = -0.07$, $P = 0.65$; Fig 2).

In global analyses, BMO-MRW yielded higher diagnostic performance than RNFLT or BMO-HRW (area under the ROC 0.96 [95% confidence interval {CI}, 0.92–1.00], 0.92 [95% CI, 0.88–0.96], and 0.85 [95% CI, 0.78–0.91], respectively). At 95% specificity, global RNFLT, BMO-HRW, and BMO-MRW yielded a sensitivity of 70%, 51%, and 81%, respectively (Fig 3), indicating that global BMO-MRW had 1.2 times higher sensitivity than global RNFLT and 1.6 times higher sensitivity than global BMO-HRW. The 2 CSLT indices MRA1 and MR2 yielded sensitivity/specificity combinations of 56%/90% and 76%/71%, respectively.

In sectoral analyses, at 95% specificity, the sensitivity of BMO-MRW was consistently higher than either of the SD-OCT or CSLT indices (Fig 4), except the superonasal quadrant where RNFLT had a higher sensitivity (59% compared with 54%). At 95% specificity, the sensitivity of BMO-MRW varied from 54% (superonasal) to 79% (inferotemporal). The corresponding figures for RNFLT and BMO-HRW were 31% (nasal) to 59% (superonasal and inferotemporal) and 35% (superonasal and temporal) to 64% (superotemporal), respectively. At 95% specificity, the sensitivity of BMO-MRW was between 0.9 (superonasal) and 2.1 (nasal) times that of RNFLT and 1.2 (superotemporal) and 1.7 (inferonasal) times that of BMO-HRW.

Examples of patients showing the significant discordance among MRA, BMO-HRW, and BMO-MRW are shown in Figure 5. Sectorally DM-based MRA results within normal limits can occur with BMO-HRW at borderline values in the normal distribution and with BMO-MRW considerably outside normal values (Fig 5A). On the other hand, an abnormal MRA

can occur with BMO-HRW and BMO-MRW within normal limits (Fig 5B). Finally, BMO-MRW can be thin (at the 5th percentile of the normal distribution) with MRA and BMO-HRW well within normal limits (Fig 5C).

The impact of a positive or negative test result based on a cutoff value yielding 95% specificity with the SD-OCT indices is shown in Figure 6. Data for MRA1 (which yielded specificity of 90%) are shown for comparison. The posttest probability after a positive BMO-MRW increased substantially from pretest values. For example, for pretest probabilities of 1% and 10%, the posttest probabilities increased to 14% and 64%, respectively. The corresponding posttest probabilities for RNFLT, BMO-HRW, and MRA1 were 12% and 61%, 9% and 53%, and 5% and 38%, respectively. At 1% and 10% pretest probabilities, a negative test result reduced the posttest values to 0% and 2% with BMO-MRW, 0% and 3% with RNFLT, 1% and 5% with BMO-HRW, and 0% and 5% with MRA1, respectively (Fig 6).

Discussion

Current optic DM-based neuroretinal rim estimates assume that the clinically visible DM is a true anatomic border of the rim tissue from which width, area, or volume measurements of the rim can be made. We recently demonstrated that (1) the clinically visible DM is rarely a consistent anatomic structure;[2] (2) there are clinically and photographically invisible, but SD-OCT detected, portions of BM and its termination that form the true outer border of rim tissue;[2] and (3) because of (1) and (2), significant errors are present in DM-based rim tissue measurements in patients with glaucoma and healthy controls.[3]

We previously reasoned that BMO-MRW determined with SD-OCT overcomes the limitations of the current quantification of the rim in 2 ways. First, it is a measurement from an actual anatomic outer border, and second, it is a geometrically accurate measurement that is independent of arbitrary reference planes that distinguish between rim and cup.[3] In the present study, we demonstrate for the first time that the anatomic accuracy of BMO-MRW translates into significantly enhanced diagnostic capabilities.

Compared with DM-based assessment with CSLT, where rim parameters are derived horizontally in the plane of the peripheral ILM surface at a fixed depth below a portion of the DM, the diagnostic performance of BMO-MRW was substantially higher. The 2 CSLT-based MRA indices yielded discrete sensitivity/specificity combinations of 56%/90% (MRA1) and 76%/71% (MRA2) and not continuous values with which an entire ROC curve could be derived. Matched for MRA1 and MRA2 specificity, BMO-MRW yielded sensitivity of 85% and 98%, respectively, whereas matched for sensitivity, specificity was 98% and 98%, respectively.

It is important to note that BMO-HRW, the current manner in which the rim is assessed with SD-OCT,[4–6,20–22] had consistently poorer diagnostic capabilities compared with BMO-MRW, both globally and sectorally. Thus, although BMO-HRW estimates rim width from an anatomically accurate location, the geometric errors associated with not accounting for the orientation of the overlying rim tissue at the point of measurement[3] likely explains why BMO-HRW performs relatively poorly compared with BMO-MRW.

The SD-OCT–based RNFLT measurements are made approximately perpendicular to the ILM and are therefore geometrically accurate in a manner that is similar to BMO-MRW. Therefore, the diagnostic capabilities of RNFLT would be expected to be comparable to BMO-MRW. Our results show that performance of RNFLT measurements were in between those of BMO-HRW and BMO-MRW (Figs 3 and 4). There are no unequivocal explanations for why the performance of BMO-MRW and RNFLT was not more closely

matched; however, there are at least 3 possibilities. First, the magnitude and mode of tissue remodeling after neural loss may be different in the RNFL compared with the ONH where neural loss could be more accurately represented. Second, BMO-MRW may be more sensitive to ONH conformational changes that precede but do not directly correlate to RNFL loss. Third, there is imprecision of the spatial correlation between the points of measurement in the peripapillary retina and the ONH.[23] This observation is supported by the presence of overlapping and nonparallel trajectories of axon bundles at a given point of measurement in the peripapillary retina[24,25] that project to less localized points in the ONH. The latter explanation may explain the large variation among the sectors in the relative diagnostic performance of the SD-OCT indices. Data acquisition and most analyses currently assume that the angle between the ONH center and the fovea is constant among all individuals. Thus, analyses that use the same angular positions for the sectors without accounting for interindividual anatomic variations may induce variably large errors when referring to normative databases or when relating to visual field measures. Analyses strategies that account for the variations in BMO center to fovea axis have recently been suggested;[26] however, we propose additionally that all SD-OCT data acquisition should also occur with reference to the BMO center to fovea axis. Such strategies are likely to decrease the interindividual variation of normative databases, thereby potentially increasing the diagnostic precision of all parameters.

Identification of glaucomatous optic nerve damage with photographic[27,28] or modern imaging[28–32] techniques in isolation has inadequate diagnostic capability for effective screening or case identification in primary eye care because of the high false-positive rate at acceptable sensitivity. By assuming a glaucoma prevalence of 2%, the diagnostic merit of a test is affected more by specificity than sensitivity. For example, at 80% specificity, the likelihood of disease after a positive test result increases from 8% to only 9% when the sensitivity increases from 80% to 99%. Therefore, in our analyses we referenced diagnostic performance of the indices at a higher specificity value of 95% at which the sensitivity of global RNFLT, BMO-HRW, and BMO-MRW was 70%, 51%, and 81%, respectively.

The LR of a positive diagnostic test based on BMO-MRW was more than 16, indicating a large effect on disease likelihood with a positive test result.[33] If the pretest probability of glaucomatous optic neuropathy were 2%, the posttest probability would increase to 25%. If clinical history and risk factors increase the pretest probability to 5% or 10%, the likelihood of glaucoma would increase to 46% and 64%, respectively, after a positive test result. The LR of a negative test result based on BMO-MRW was 0.2, indicating a moderate effect[33] on ruling out glaucoma. The posttest probability with a negative test result at pretest probability of 2%, 5%, and 10% was 0%, 1%, and 2%, respectively.

This study has some limitations. The comparison of BMO-MRW with conventional DM-based rim measurement was performed with CLST and not stereo disc photographs. From the perspective of diagnostic precision, comparable results with disc photography and MRA have been reported,[34,35] although other studies have suggested MRA to be poorer.[36]

Healthy controls were on average 5 years younger than the patients, possibly resulting in a more favorable diagnostic performance of the indices evaluated. However, the age difference would not affect the relative comparison of the indices. The cutoff values used to achieve 95% specificity at which comparison of the SD-OCT indices were made were obtained in the same sample, whereas the MRA cutoffs were derived from an independent population. Thus, again, although the relative comparison of the SD-OCT indices is valid, the cutoffs from this study applied to other populations may result in different diagnostic performances.

Segmentation of BMO and the ILM was performed manually. Although the mean reproducibility of BMO-MRW calculations in preliminary analyses is high (yielding an average paired difference of 0.7%), the manual segmentations are time-consuming. Investigators have described automated segmentation of several structures in the SD-OCT B-scan;[4,5] however, we are unaware of systematic verification of these methods. Recent work suggests that a newly developed automated algorithm for BMO and ILM segmentation, and BMO-MRW calculation is accurate (AlMobarak FA, O'Leary N, Sharpe GP, et al. Invest Ophthalmol Vis Sci 2012;53:E-abstract 691); therefore, it is possible for the analyses described in this study to be incorporated into current acquisition and analysis software.

In conclusion, we have previously reasoned that the foundation of current optic DM-based neuroretinal rim assessment lacks a justifiable anatomic and geometric rationale.[2,3] The BMO-MRW is a measurement from an anatomically accurate border of the rim that also takes into account its varying trajectory relative to the point of measurement. In this study, we showed that BMO-MRW also has better diagnostic performance compared with current CSLT or SD-OCT–-based ONH and RNFLT parameters. Further studies are now necessary to incorporate this parameter with other clinical markers to enhance the detection and risk profiling of glaucoma, and to evaluate its performance in the detection of progression.

Acknowledgments

Financial Disclosure(s):

The author(s) have made the following disclosure(s): B.C.C. and C.F.B. received grant support from Heidelberg Engineering.

Grants MOP11357 (B.C.C.) from the Canadian Institutes of Health Research, Ottawa, Ontario; Capes Foundation (A.S.C.R.), Ministry of Education of Brazil, Brasilia, Brazil; US Public Health Service Grants R01EY011610 (C.F.B.) from the National Eye Institute, National Institutes of Health, Bethesda, Maryland; The Legacy Good Samaritan Foundation (C.F.B.), Portland, Oregon; the Sears Trust for Biomedical Research (C.F.B.), Mexico, Missouri; the Alcon Research Institute (C.F.B.), Fort Worth, Texas; and equipment and unrestricted research support from Heidelberg Engineering (B.C.C., C.F.B.), Heidelberg, Germany.

References

1. Hogan, MJ.; Alvarado, JA.; Weddell, JE. Histology of the Human Eye: An Atlas and Textbook. Philadelphia, PA: Saunders; 1971. p. 538-540.
2. Reis AS, Sharpe GP, Yang H, et al. Optic disc margin anatomy in patients with glaucoma and normal controls with spectral domain optical coherence tomography. Ophthalmology. 2012; 119:738–747. [PubMed: 22222150]
3. Reis AS, O'Leary N, Yang H, et al. Influence of clinically invisible, but optical coherence tomography detected, optic disc margin anatomy on neuroretinal rim evaluation. Invest Ophthalmol Vis Sci. 2012; 53:1852–1860. [PubMed: 22410561]
4. Abramoff MD, Lee K, Niemeijer M, et al. Automated segmentation of the cup and rim from spectral domain OCT of the optic nerve head. Invest Ophthalmol Vis Sci. 2009; 50:5778–5784. [PubMed: 19608531]
5. Hu Z, Abramoff MD, Kwon YH, et al. Automated segmentation of neural canal opening and optic cup in 3D spectral optical coherence tomography volumes of the optic nerve head. Invest Ophthalmol Vis Sci. 2010; 51:5708–5717. [PubMed: 20554616]
6. Lee K, Niemeijer M, Garvin MK, et al. Segmentation of the optic disc in 3-D OCT scans of the optic nerve head. IEEE Trans Med Imaging. 2010; 29:159–168. [PubMed: 19758857]
7. Mwanza JC, Chang RT, Budenz DL, et al. Reproducibility of peripapillary retinal nerve fiber layer thickness and optic nerve head parameters measured with Cirrus HD-OCT in glaucomatous eyes. Invest Ophthalmol Vis Sci. 2010; 51:5724–5730. [PubMed: 20574014]

8. Chen TC. Spectral domain optical coherence tomography in glaucoma: qualitative and quantitative analysis of the optic nerve head and retinal nerve fiber layer (an AOS thesis). Trans Am Ophthalmol Soc. 2009; 107:254–281. [PubMed: 20126502]
9. Povazay B, Hofer B, Hermann B, et al. Minimum distance mapping using three-dimensional optical coherence tomography for glaucoma diagnosis. J Biomed Opt. 2007; 12:041204. [PubMed: 17867793]
10. Strouthidis NG, Fortune B, Yang H, et al. Longitudinal change detected by spectral domain optical coherence tomography in the optic nerve head and peripapillary retina in experimental glaucoma. Invest Ophthalmol Vis Sci. 2011; 52:1206–1219. [PubMed: 21217108]
11. Chauhan BC, Hutchison DM, Artes PH, et al. Optic disc progression in glaucoma: comparison of confocal scanning laser tomography to optic disc photographs in a prospective study. Invest Ophthalmol Vis Sci. 2009; 50:1682–1691. [PubMed: 19060290]
12. Chauhan BC, Nicolela MT, Artes PH. Incidence and rates of visual field progression after longitudinally measured optic disc change in glaucoma. Ophthalmology. 2009; 116:2110–2118. [PubMed: 19500850]
13. Åsman P, Heijl A. Glaucoma Hemifield Test. Automated visual field evaluation. Arch Ophthalmol. 1992; 110:812–819. [PubMed: 1596230]
14. Bengtsson B, Olsson J, Heijl A, Rootzen H. A new generation of algorithms for computerized threshold perimetry, SITA. Acta Ophthalmol Scand. 1997; 75:368–375. [PubMed: 9374242]
15. Langenegger SJ, Funk J, Toteberg-Harms M. Reproducibility of retinal nerve fiber layer thickness measurements using the eye tracker and the retest function of Spectralis SD-OCT in glaucomatous and healthy control eyes. Invest Ophthalmol Vis Sci. 2011; 52:3338–3344. [PubMed: 21330656]
16. Strouthidis NG, Yang H, Downs JC, Burgoyne CF. Comparison of clinical and three-dimensional histomorphometric optic disc margin anatomy. Invest Ophthalmol Vis Sci. 2009; 50:2165–2174. [PubMed: 19136694]
17. Strouthidis NG, Yang H, Fortune B, et al. Detection of optic nerve head neural canal opening within histomorphometric and spectral domain optical coherence tomography data sets. Invest Ophthalmol Vis Sci. 2009; 50:214–223. [PubMed: 18689697]
18. Wollstein G, Garway-Heath DF, Hitchings RA. Identification of early glaucoma cases with the scanning laser ophthalmoscope. Ophthalmology. 1998; 105:1557–1563. [PubMed: 9709774]
19. Sackett, DL.; Haynes, RB.; Guyatt, GH.; Tugwell, P. Clinical Epidemiology: A Basic Science for Clinical Medicine. 2nd ed.. Boston, MA: Little, Brown; 1991. p. 119-139.
20. Mwanza JC, Oakley JD, Budenz DL, Anderson DR. Cirrus Optical Coherence Tomography Normative Database Study Group. Ability of Cirrus HD-OCT optic nerve head parameters to discriminate normal from glaucomatous eyes. Ophthalmology. 2011; 118:241–248. [PubMed: 20920824]
21. Rao HL, Leite MT, Weinreb RN, et al. Effect of disease severity and optic disc size on diagnostic accuracy of RTVue spectral domain optical coherence tomograph in glaucoma. Invest Ophthalmol Vis Sci. 2011; 52:1290–1296. [PubMed: 20811060]
22. Resch H, Deak G, Pereira I, Vass C. Comparison of optic disc parameters using spectral domain Cirrus high-definition optical coherence tomography and confocal scanning laser ophthalmoscopy in normal eyes [report online]. Acta Ophthalmol. 2012; 90:e225–e229. [PubMed: 22458635]
23. Jansonius NM, Nevalainen J, Selig B, et al. A mathematical description of nerve fiber bundle trajectories and their variability in the human retina. Vision Res. 2009; 49:2157–2163. [PubMed: 19539641]
24. Jeoung JW, Kim TW, Kang KB, et al. Overlapping of retinal nerve fibers in the horizontal plane. Invest Ophthalmol Vis Sci. 2008; 49:1753–1757. [PubMed: 18436809]
25. Burk RO, Tuulonen A, Airaksinen PJ. Laser scanning tomography of localised nerve fibre layer defects. Br J Ophthalmol. 1998; 82:1112–1117. [PubMed: 9924295]
26. Patel NB, Wheat JL, Rodriguez A, et al. Agreement between retinal nerve fiber layer measures from Spectralis and Cirrus spectral domain OCT [report online]. Optom Vis Sci. 2012; 89:E652–E666. [PubMed: 22105330]

27. Abrams LS, Scott IU, Spaeth GL, et al. Agreement among optometrists, ophthalmologists, and residents in evaluating the optic disc for glaucoma. Ophthalmology. 1994; 101:1662–1667. [PubMed: 7936564]

28. Deleon-Ortega JE, Arthur SN, McGwin G Jr, et al. Discrimination between glaucomatous and nonglaucomatous eyes using quantitative imaging devices and subjective optic nerve head assessment. Invest Ophthalmol Vis Sci. 2006; 47:3374–3380. [PubMed: 16877405]

29. Ford BA, Artes PH, McCormick TA, et al. Comparison of data analysis tools for detection of glaucoma with the Heidelberg Retina Tomograph. Ophthalmology. 2003; 110:1145–1150. [PubMed: 12799239]

30. Saito H, Tomidokoro A, Yanagisawa M, et al. Sensitivity and specificity with the glaucoma probability score in Heidelberg Retina Tomograph II in Japanese eyes. J Glaucoma. 2009; 18:227–232. [PubMed: 19295378]

31. Healey PR, Lee AJ, Aung T, et al. Diagnostic accuracy of the Heidelberg Retina Tomograph for glaucoma: a population-based assessment. Ophthalmology. 2010; 117:1667–1673. [PubMed: 20816247]

32. Greaney MJ, Hoffman DC, Garway-Heath DF, et al. Comparison of optic nerve imaging methods to distinguish normal eyes from those with glaucoma. Invest Ophthalmol Vis Sci. 2002; 43:140–145. [PubMed: 11773024]

33. Jaeschke R, Guyatt GH, Sackett DL. Users' guides to the medical literature. III. How to use an article about a diagnostic test. B. What are the results and will they help me in caring for my patients? JAMA. 1994; 271:703–707. [PubMed: 8309035]

34. Reus NJ, de Graaf M, Lemij HG. Accuracy of GDx VCC, HRT I, and clinical assessment of stereoscopic optic nerve head photographs for diagnosing glaucoma. Br J Ophthalmol. 2007; 91:313–318. [PubMed: 17035283]

35. Pablo LE, Ferreras A, Fogagnolo P, et al. Optic nerve head changes in early glaucoma: a comparison between stereophotography and Heidelberg retina tomography. Eye (Lond). 2010; 24:123–130. [PubMed: 19218992]

36. Girkin CA, DeLeon-Ortega JE, Xie A, et al. Comparison of the Moorfields classification using confocal scanning laser ophthalmoscopy and subjective optic disc classification in detecting glaucoma in blacks and whites. Ophthalmology. 2006; 113:2144–2149. [PubMed: 16996609]

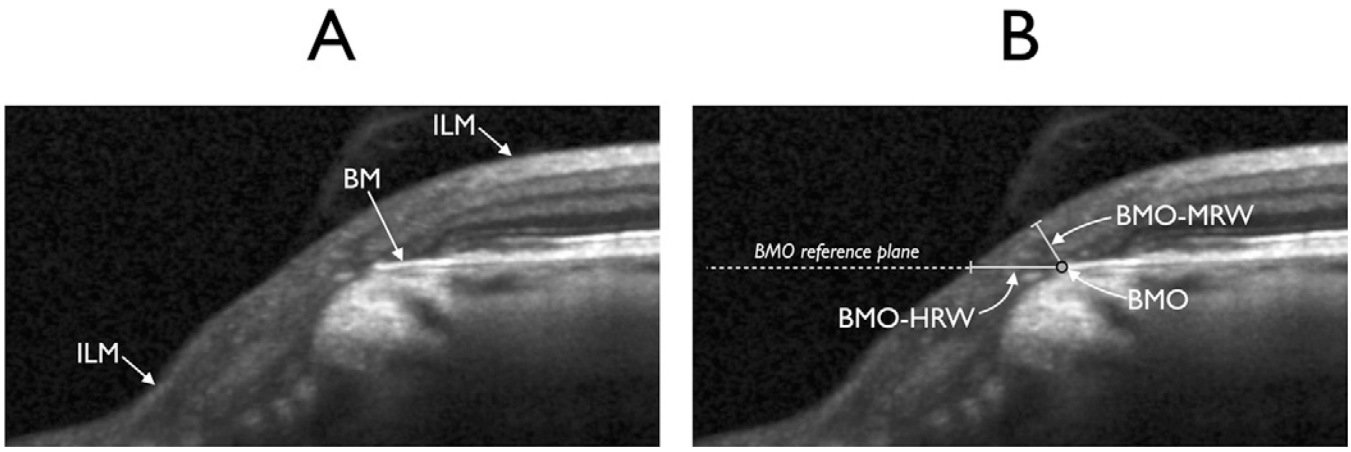

Figure 1.

Neuroretinal rim parameters measured with spectral-domain optical coherence tomography (SD-OCT). **A**, Portion of a radial B-scan illustrating Bruch's membrane (BM) and internal limiting membrane (ILM). **B**, Same portion of the B-scan illustrating Bruch's membrane opening (BMO), BMO-horizontal rim width (BMO-HRW), the distance from BMO to the ILM along the BMO reference plane, and Bruch's membrane opening-minimum rim width (BMO-MRW), the minimum distance from BMO to the ILM.

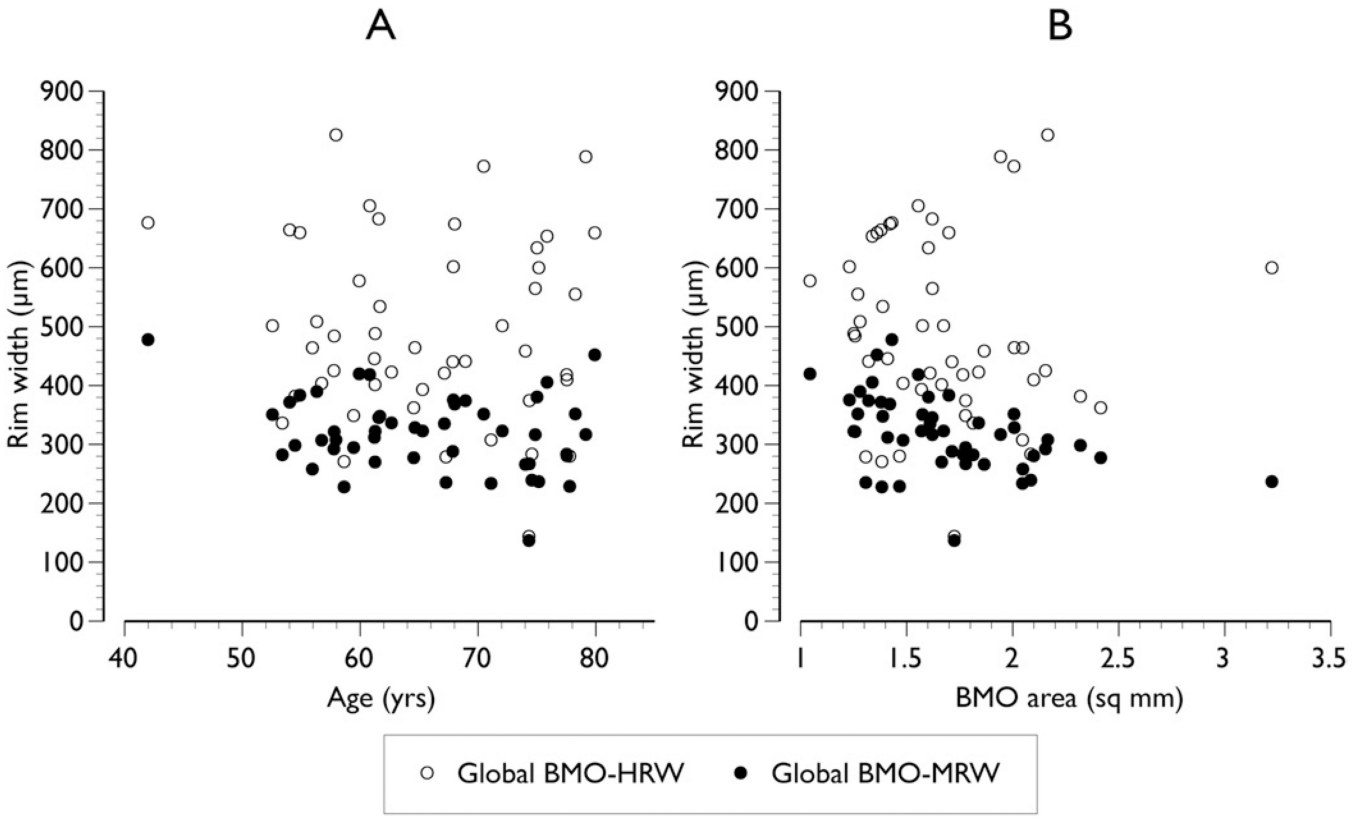

Figure 2.
Relationship between the 2 Bruch's membrane opening (BMO)–based parameters, Bruch's membrane opening-horizontal rim width (BMO-HRW) and Bruch's membrane opening-minimum rim width (BMO-MRW), and age **(A)** and BMO area **(B)** in healthy control subjects.

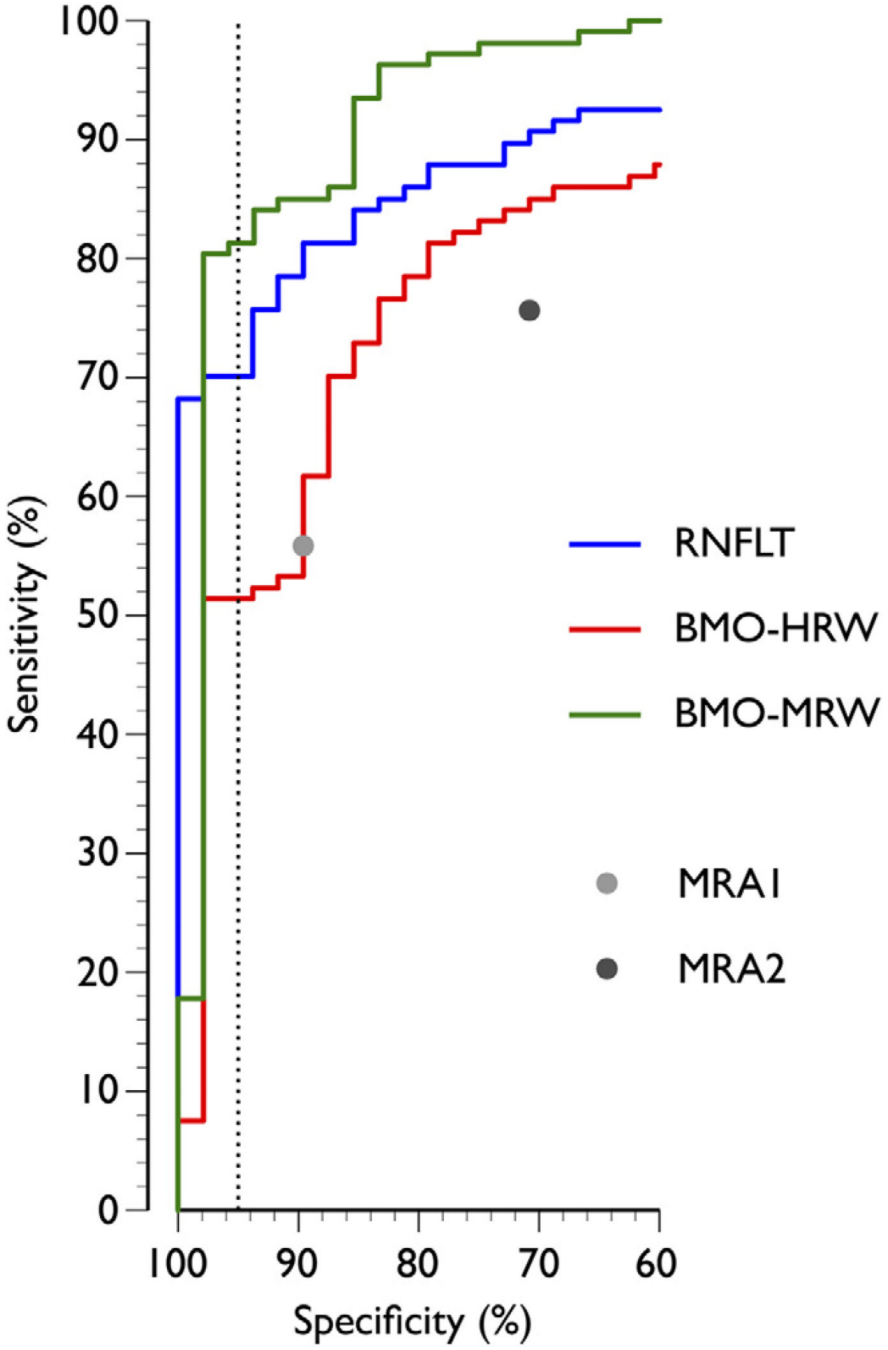

Figure 3.

The receiver operating characteristic (ROC) curves illustrating the diagnostic performance of retinal nerve fiber layer thickness (RNFLT), Bruch's membrane opening-horizontal rim width (BMO-HRW), and Bruch's membrane opening-minimum rim width (BMO-MRW) computed globally. Also shown are the 2 discrete points of the global Moorfields Regression Analysis (MRA) from confocal scanning laser tomography (CSLT), MRA1 where "borderline" cases were classified as normal, and MRA2 where "borderline" cases were classified as abnormal. *Dashed vertical line* indicates specificity of 95%.

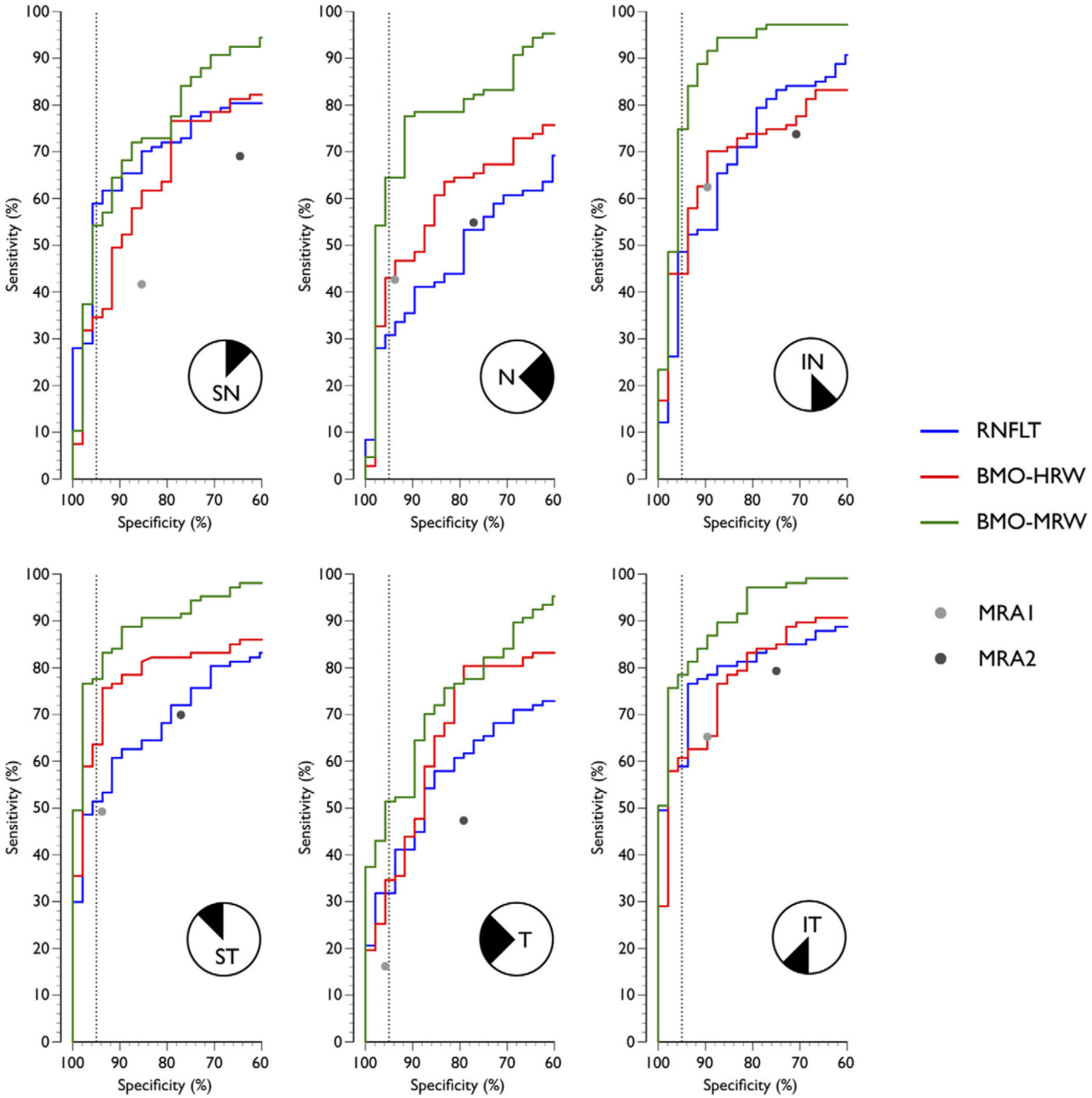

Figure 4.

The confocal scanning laser tomography (ROC) curves illustrating the diagnostic performance of retinal nerve fiber layer thickness (RNFLT), Bruch's membrane opening-horizontal rim width (BMO-HRW), and Bruch's membrane opening-minimum rim width (BMO-MRW) computed for the 6 sectors. Also shown are the 2 discrete points of the sectoral Moorfields Regression Analysis (MRA) from confocal scanning laser tomography (CSLT), conservative Moorfields Regression Analysis (MRA1) where "borderline" cases were classified as normal, and liberal Moorfields Regression Analysis (MRA2) where "borderline" cases were classified as abnormal. *Dashed vertical line* indicates specificity of

95%. IN = inferonasal; IT = inferotemporal; N = nasal; SN = superonasal; ST = superotemporal; T = temporal.

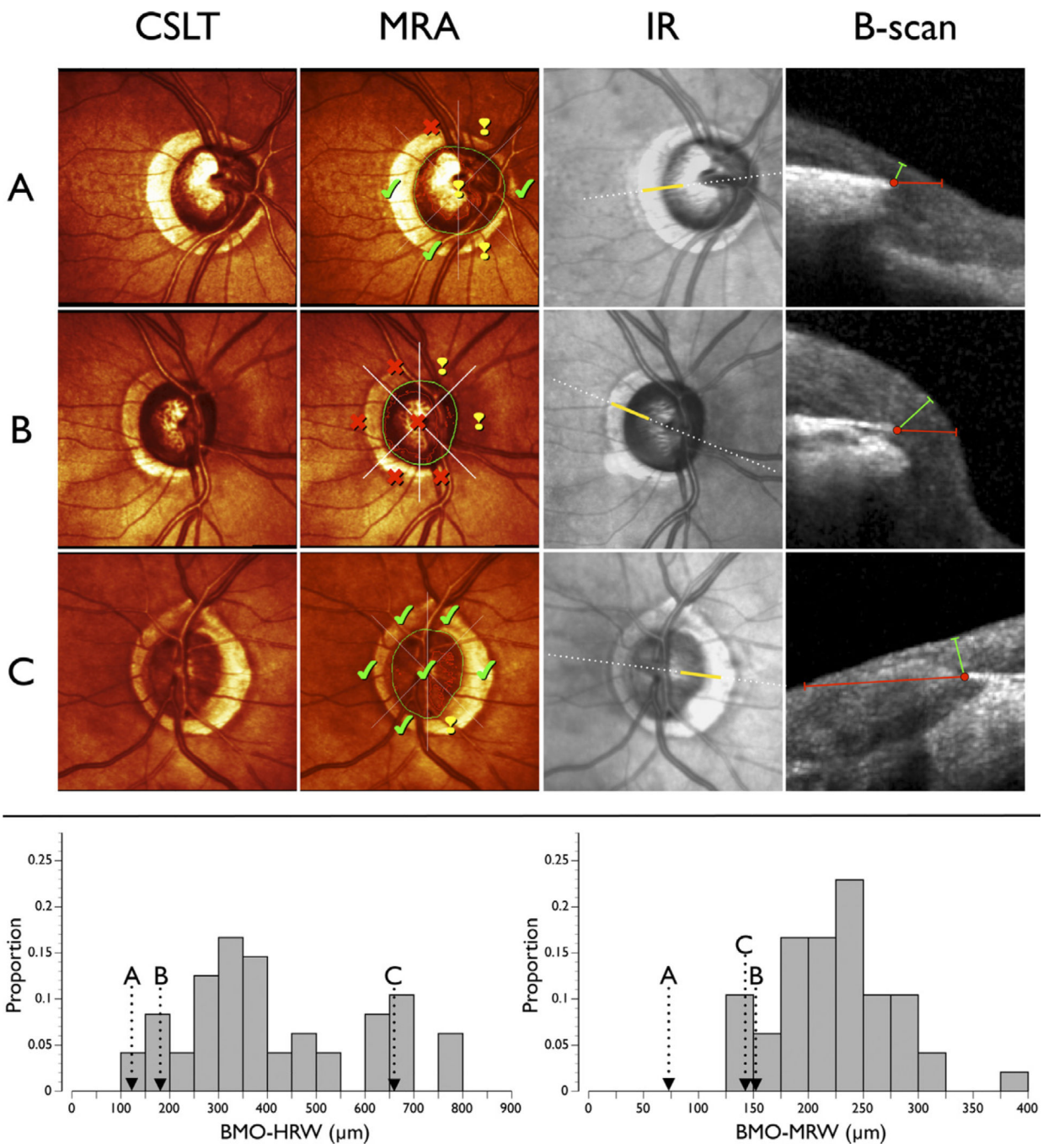

Figure 5.

Examples of patients with glaucoma illustrating the significant discordance between results of confocal scanning laser tomography (CSLT) and spectral-domain optical coherence tomography (SD-OCT). CSLT, pseudocolor optic nerve head (ONH) image; Moorfields Regression Analysis (MRA), results from the MRA where the *closed green shape* represents the clinical optic disc margin (DM). The MRA results indicate “within normal limits” (*check mark*), “borderline” (*exclamation mark*), and “outside normal limits” (*cross*) for each of the 6 sectors and globally. Infrared (IR) image from SD-OCT where the *dotted white line* indicates the position of the radial B-scan (shown in the next column). B-scan, portion of the B-scan (indicated by the *solid yellow line* in the previous column). *Red dot* shows BMO, *red*

line shows Bruch's membrane opening-horizontal rim width (BMO-HRW), and *green line* shows Bruch's membrane opening-minimum rim width (BMO-MRW). *Bottom:* distribution of temporal BMO-HRW (*left*) and temoporal BMO-MRW (*right*) in healthy control subjects. **A**, Right ONH of a patient with MRA within normal limits in the temporal sector. The mean temporal BMO-HRW is less than the 5th percentile of the normal distribution (*arrow*), whereas the BMO-MRW value is less than half of the lowest value in the normal distribution. **B**, Right ONH of a patient with MRA outside normal limits in the temporal sector. The mean temporal BMO-HRW and BMO-MRW are approximately the 10th percentile of the normal distribution. **C**, Left ONH of a patient with MRA within normal limits in the temporal sector. The mean temporal BMO-HRW is approximately the 85th percentile of the normal distribution, but the mean temporal BMO-MRW is approximately the 5th percentile of the normal distribution.

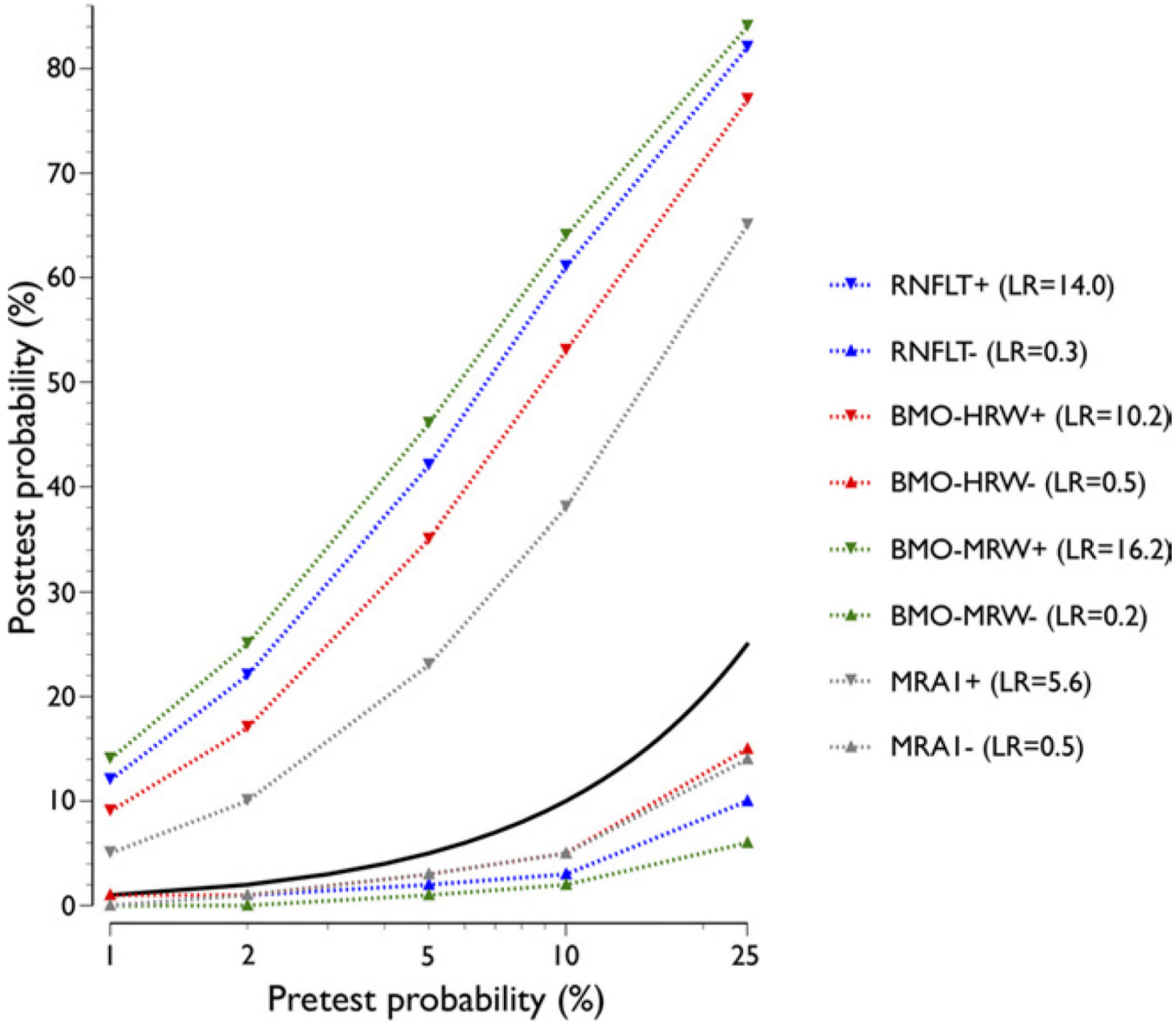

Figure 6.

Pre- and posttest probability of the various global parameters based on cutoff values yielding 95% specificity. Data comparing circumpapillary retinal nerve fiber layer thickness (RNFLT), Bruch's membrane opening-horizontal rim width (BMO-HRW), and Bruch's membrane opening-minimum rim width (BMO-MRW) and the more conservative conservative Moorfields Regression Analysis (MRA) cutoff (MRA1), which yields 90% specificity, are shown. Posttest probabilities for both positive (+) and negative (−) test results are indicated. The likelihood ratio (LRs) for positive and negative test results are shown. *Solid black line* indicates equal pre- and posttest probability.

Table 1

Summary of Spectral-Domain Optical Coherence Tomography Parameters in Patients with Glaucoma and Healthy Controls*

	Patients with Glaucoma	Healthy Controls
BMO area (mm^2)	1.8 (1.6–2.1)	1.7 (1.4–1.9)
Circumpapillary RNFLT (μm)	70.0 (63.2–80.0)	95.9 (91.1–103.5)
Global BMO-HRW (μm)	253.1 (189.5–352.1)	461.7 (392.8–623.1)
Global BMO-MRW (μm)	182.7 (142.2–217.7)	316.5 (275.4–361.7)

BMO = Bruch's membrane opening; BMO-HRW = Bruch's membrane opening-horizontal rim width; BMO-MRW = Bruch's membrane opening-minimum rim width; RNFLT = retinal nerve fiber layer thickness.

*Values shown are medians (interquartile range).